coatings

MDPI

Article

Study on the Adhesion Performance of Biochar-Modified Asphalt Based on Surface Free Energy and Atomic Force Microscopy

Quan Li [1,2], Le Xu [1], Xing Chen [3], Wen Li [1], Yongwei Li [4], Hanqing Wang [1,*] and Kefei Liu [1,*]

[1] School of Civil Engineering, Central South University of Forestry & Technology, Changsha 410004, China; 20220100061@csuft.edu.cn (Q.L.); 20221100418@csuft.edu.cn (L.X.); t20222710@csuft.edu.cn (W.L.)
[2] Hunan Province Research and Construction Center for Building Solid Waste Utilization Technology, Changsha 410083, China
[3] Hunan Expressway Engineering Consulting Co., Ltd., Changsha 410329, China; 20221200554@csuft.edu.cn
[4] School of Civil Engineering, Central South University, Changsha 410083, China; yongweili@csu.edu.cn
* Correspondence: hqwang@csuft.edu.cn (H.W.); t20081741@csuft.edu.cn (K.L.)

Abstract: To investigate the effect of biochar on the adhesion performance of asphalt, the macroscopic and microscopic adhesion performance of 70# base asphalt, SBS-modified asphalt (SBSMA), sludge-based biochar-modified asphalt, and waste wood-based biochar-modified asphalt (WWBMA) were tested using atomic force microscopy (AFM) and contact angle tests, respectively. The impact of these two testing methods on the evaluation of adhesion performance was also analyzed. Research results indicated that biochar increased the number of bee-like structures on the asphalt surface while significantly reducing their average area. This improves the distribution of asphalt adhesion by reducing the adhesion difference between bee-like structured areas and non-bee-like structured areas while simultaneously enhancing the overall adhesion of the asphalt surface. Surface free energy (SFE) theory analysis indicates a linear correlation between the SFE obtained from the contact angle test and the atomic force microscopy test. Biochar significantly increases the SFE of asphalt and its components, thereby increasing the work of adhesion between asphalt and aggregate and reducing the work of debonding. Consequently, it improves the bonding performance between asphalt and aggregate, as well as its resistance to moisture damage.

Keywords: biochar-modified asphalt (BMA); adhesion; surface free energy (SFE); atomic force microscopy

Citation: Li, Q.; Xu, L.; Chen, X.; Li, W.; Li, Y.; Wang, H.; Liu, K. Study on the Adhesion Performance of Biochar-Modified Asphalt Based on Surface Free Energy and Atomic Force Microscopy. *Coatings* **2024**, *14*, 1390. https://doi.org/10.3390/coatings14111390

Academic Editor: Edoardo Proverbio

Received: 30 September 2024
Revised: 29 October 2024
Accepted: 29 October 2024
Published: 31 October 2024

1. Introduction

In recent years, with the accelerated pace of urbanization in China, the production of municipal sewage sludge has been increasing year by year. Many large cities face social issues such as large amounts of untreated sewage sludge, low resource utilization rates, and severe environmental pollution [1,2]. Producing biochar from sludge can achieve sludge stabilization and harmless treatment. Biochar can improve the high-temperature stability and anti-aging performance of asphalt binders, as well as enhance the rutting resistance of asphalt mixtures [3–5]. The adhesion performance of biochar-modified asphalt (BMA) is directly related to the moisture damage resistance and durability of asphalt mixtures. However, systematic and in-depth research on this subject is still lacking. Therefore, exploring the impact of biochar on asphalt adhesion performance is of significant importance.

Many scholars, both domestically and internationally, have used atomic force microscopy (AFM) to study the adhesion performance of asphalt. However, there are differing views regarding the chemical structure of the bee-like structures on the microscopic surface of asphalt, and researchers have drawn different conclusions based on the variations in the microscopic structure of the asphalt surface. Loeberr [6] suggested that the "bee-like structures" are formed by the aggregation of asphaltenes on the surface, and Wu Shaopeng

et al. [7,8] also concluded that the bee-like structures result from the aggregation of asphaltenes on the surface. However, in recent years, more scholars have attributed the formation of bee-like structures to wax crystallization, arguing that at low temperatures, the wax components aggregate and crystallize with asphaltenes, ultimately forming the bee-like structures [9,10]. Pauli et al. [11] used AFM to scan the microscopic surface structure of asphalt containing different components and found that bee-like structures existed on the microscopic surface of asphalt without asphaltenes. However, after the removal of wax components, the bee-like structures disappeared. When different types of solid wax and microcrystalline wax were added to asphalt from which asphaltenes had been removed, various forms of bee-like structures reappeared on the asphalt surface. Therefore, Pauli et al. hypothesized that the interaction between wax crystallization and asphalt components is the primary cause of the formation of bee-like structures, and they referred to this process as "wax-induced phase separation". Das et al. [12] prepared AFM asphalt samples using a thermal melting method to investigate the phase separation on the microscopic surface of three base asphalts from different sources and one sand wax-modified asphalt at different test temperatures, correlating the results with differential scanning calorimetry (DSC). The results indicated that phase separation was associated with the wax components in asphalt. Additionally, Das et al. [13] used a mechanical property measurement mode based on peak force tapping (AFM-QNM) to study the effect of different aging forms on the microscopic adhesion force of asphalt. The results showed that aging reduced the adhesion force of asphalt. Pang [14] studied the changes in the microscopic surface structure of different asphalts after short-term and long-term aging. The findings revealed that, before aging, the bee-like structures on the asphalt surface were dispersed. After short-term aging, the bee-like structures began to aggregate, and after long-term aging, the number of bee-like structures continued to decrease, with aggregation further intensifying. Liu et al. [15] found that the microscopic surface of asphalt becomes rougher after aging. Laurell et al. [16] used the QNM mode to investigate the microscopic surface morphology and mechanical properties of base asphalt. The results showed that the distribution of the microscopic surface morphology was consistent with the distribution of mechanical properties, with the adhesion force in the bee-like structures and their surrounding areas being lower than in other flat regions.

Existing studies have shown that AFM, as a powerful tool with nanometer resolution, could enable analysis of the microscopic morphology and mechanical properties of asphalt at the nanoscale. Meanwhile, the use of QNM technology allows for the simultaneous acquisition of microscopic surface morphology and various mechanical properties, as well as their distribution. This makes it a powerful method for investigating the effects of biochar on the microscopic structure and mechanical properties of asphalt.

Currently, the impact of biochar on the adhesion performance of asphalt binders, especially its influence on the microscopic mechanical properties and their distribution, remains unclear. Moreover, there is a lack of reasonable explanation regarding the relationship between the microscopic effects of biochar on the adhesion performance of asphalt binders and their macroscopic performance in practical applications. Therefore, the main objective of this study is to quantify the effects of biochar on the microscopic morphology, mechanical properties, and their distribution in asphalt binders, establish the connection between the microscopic mechanical properties affected by biochar and the macroscopic adhesion performance, and reveal the underlying mechanisms through which biochar influences the adhesion performance of asphalt binders. In this study, AFM tests and contact angle measurements were conducted to assess the macro- and microscopic adhesion performance of 70# base asphalt, SBS-modified asphalt (SBSMA), sludge-based biochar-modified asphalt (SBMA), and waste wood-based biochar-modified asphalt (WWBMA). The findings provide valuable insights into the water damage resistance of BMA and offer a theoretical foundation and data support for the application of biochar in asphalt mixtures.

2. Surface Free Energy Theory (SFE)

Surface free energy (SFE) refers to the work performed to increase the unit surface area of a material under vacuum conditions by the application of external forces. The greater the SFE, the more energy is released when a new surface is formed, resulting in a tighter bond on the new surface. Generally, the larger the SFE of asphalt, the stronger its adhesion performance. SFE is primarily composed of non-polar dispersion components and polar acid-base components. Its calculation expression is shown in Equation (1) [17,18]:

$$\gamma = \gamma^{LW} + \gamma^{AB} = \gamma^{LW} + 2\sqrt{\gamma^{+}\gamma^{-}} \tag{1}$$

In the equation, γ^{LW} represents the non-polar dispersion component, mJ/m^2; γ^{AB} represents the polar acid-base component, mJ/m^2; γ^{+} represents the polar acid component, mJ/m^2, and γ^{-} represents the polar base component, mJ/m^2.

From a thermodynamic perspective, the relationship between SFE parameters and bond energy, i.e., the SFE and bond energy between two phases (i, j), can be expressed by Equation (2) [17,18]:

$$\Delta G_{ij} = \gamma_{ij} - \gamma_i - \gamma_j \tag{2}$$

In the equation, ΔG_{ij} represents the interfacial bond energy between the two phases, mJ/m^2; γ_{ij} represents the interfacial SFE between the two phases, mJ/m^2; γ_i represents the SFE of material i, mJ/m^2, and γ_j represents the SFE of material j, mJ/m^2.

The relationship between the dispersion component of the interfacial bond energy between two phases and the dispersion component of the SFE of the two materials can be expressed by Equation (3) [17,18]:

$$\Delta G_{ij}^{LW} = -2\sqrt{\gamma_i^{LW}\gamma_j^{LW}} \tag{3}$$

In the equation, ΔG_{ij}^{LW} represents the dispersion component of the interfacial bond energy between the two phases, mJ/m^2; γ_i^{LW} represents the dispersion component of the SFE of material i, mJ/m^2, and γ_j^{LW} represents the dispersion component of the SFE of material j, mJ/m^2.

Unlike non-polar van der Waals interactions, polar interactions involve the interaction between electron acceptors and electron donors. Distinct from the interaction relationship of the non-polar dispersion component, the relationship between the polar component of the interfacial bond energy between two phases and the polar component of the SFE of the two materials can be expressed by Equation (4) [17,18]:

$$\Delta G_{ij}^{AB} = -2\left(\sqrt{\gamma_i^{+}\gamma_j^{-}} + \sqrt{\gamma_i^{-}\gamma_j^{+}}\right) \tag{4}$$

In the equation, ΔG_{ij}^{AB} represents the polar component of the interfacial bond energy between the two phases, mJ/m^2; γ_i^{+} represents the polar acid component of the SFE of material i, mJ/m^2; γ_i^{-} represents the polar base component of the SFE of material i, mJ/m^2; γ_j^{-} represents the polar acid component of the SFE of material j, mJ/m^2, and γ_j^{+} represents the polar base component of the SFE of material j, mJ/m^2.

Combining Equations (1) to (4), we obtain

$$\gamma_{ij} = \gamma_i + \gamma_j - 2\sqrt{\gamma_i^{LW}\gamma_j^{LW}} - 2\left(\sqrt{\gamma_i^{+}\gamma_j^{-}} + \sqrt{\gamma_i^{-}\gamma_j^{+}}\right) \tag{5}$$

By combining the method for calculating solid SFE with the Young–Dupre equation, the work of adhesion between a solid and a liquid can be obtained, as expressed by Equation (6) [19,20]:

$$W_{SL} = (1 + \cos\theta)\gamma_L = 2\sqrt{\gamma_S^{LW}\gamma_L^{LW}} + 2\left(\sqrt{\gamma_S^{+}\gamma_L^{-}} + \sqrt{\gamma_S^{-}\gamma_L^{+}}\right) \tag{6}$$

In the equation, W_{SL} represents the work of adhesion between the solid and the liquid, mJ/m^2; θ is the contact angle between the solid and the liquid, °; γ_S^{LW} is the dispersion component of the SFE of the solid, mJ/m^2; γ_L^{LW} is the dispersion component of the SFE of the liquid, mJ/m^2; γ_S^+ is the polar acid component of the SFE of the solid, mJ/m^2; γ_S^- is the polar base component of the SFE of the solid, mJ/m^2; γ_L^- is the polar acid component of the SFE of the liquid, mJ/m^2, and γ_L^+ is the polar base component of the SFE of the liquid, mJ/m^2.

When water is present, it will spontaneously displace asphalt from the aggregate surface. At this point, the interfacial bond energy at the asphalt–aggregate–water three-phase interface is denoted by ΔG_{ikj} [21], and its calculation method is shown in Equation (7):

$$\Delta G_{ikj} = \gamma_{ij} - \gamma_{ik} - \gamma_{jk} \tag{7}$$

In the equation, ΔG_{ikj} represents the interfacial bond energy between the three-phase materials, mJ/m^2; γ_{ik} represents the interfacial bond energy between the two materials i and k, mJ/m^2, and γ_{jk} represents the interfacial bond energy between the two materials j and k, mJ/m^2.

By combining Equations (1) to (7), the work of debonding between asphalt and aggregate under water immersion conditions can be obtained [21], and its calculation method is shown in Equation (8):

$$W_{a\omega s} = 2\left[\begin{array}{l} \sqrt{\gamma_a^{LW}\gamma_\omega^{LW}} + \sqrt{\gamma_s^{LW}\gamma_\omega^{LW}} + \sqrt{\gamma_\omega^+}\left(\sqrt{\gamma_a^-} + \sqrt{\gamma_s^-}\right) + \sqrt{\gamma_\omega^-}\left(\sqrt{\gamma_a^+} + \sqrt{\gamma_s^+}\right) \\ -\gamma_\omega^{LW} - \sqrt{\gamma_a^{LW}\gamma_s^{LW}} - 2\sqrt{\gamma_\omega^+\gamma_\omega^-} - 2\sqrt{\gamma_a^+\gamma_s^-} - 2\sqrt{\gamma_a^-\gamma_s^+} \end{array} \right] \tag{8}$$

In the equation, W_{aws} represents the work of adhesion between the solid and the liquid, mJ/m^2; γ_a^{LW}, γ_a^+, and γ_a^- represent the dispersion component, polar acid component, and the polar base component of the SFE of asphalt, respectively, mJ/m^2; γ_ω^{LW}, γ_ω^+, and γ_ω^- represent the dispersion component, polar acid component, and the polar base component of the SFE of water, respectively, mJ/m^2; γ_s^{LW}, γ_s^+, and γ_s^- represent the dispersion component, polar acid component, and polar base component of the SFE of the aggregate, respectively, mJ/m^2.

SFE theory is an important framework for evaluating the adhesion performance of asphalt. In this study, AFM and a contact angle measuring instrument were used to test 70# base asphalt, SBSMA, SBSMA, and WWBMA. By investigating SFE, adhesion force, and other indicators, the impact of biochar on the adhesion performance of asphalt was explored. Additionally, the differences in SFE obtained from the two testing methods were compared, and the influence of different testing methods on the evaluation of adhesion performance was analyzed.

3. Materials and Test Methods

3.1. Materials

3.1.1. Biochar

The biochar used in this study includes laboratory-made sludge-based biochar and waste wood-based biochar. The sludge was sourced from a municipal wastewater treatment plant in Changsha, Hunan, while the waste wood was collected from a construction site in Changsha. Biochar was prepared by pyrolysis using a tube furnace, with the preparation process shown in Figure 1, the appearance of the biochar in Figure 2, and the basic technical specifications of the biochar listed in Table 1.

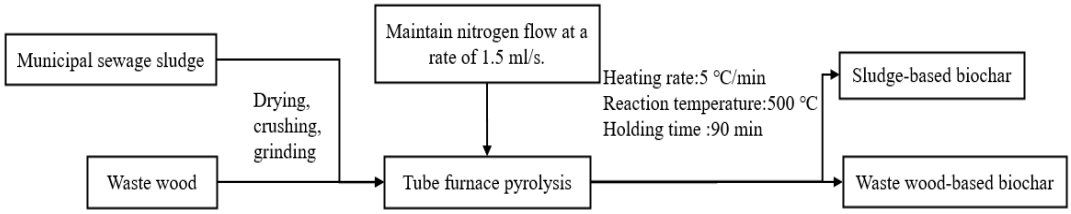

Figure 1. Biochar preparation process.

(**a**) Sludge-based biochar; (**b**) Waste wood-based biochar

Figure 2. Appearance and morphology of biochar.

Table 1. Basic technical specifications of biochar.

Types	Appearance	Particle Size/μm	Moisture Content/%	Carbon Content/%
Sludge-based biochar	Powder form	<75	4.2	24.15
Waste wood-based biochar	Powder form	<75	5.8	74.84

3.1.2. Asphalt

In this study, domestically produced Grade A 70# base asphalt (Changsha, China) and Shell SBSMA (Guangzhou, China) were used, with their main technical specifications listed in Table 2. As shown in Table 2, the performance of each asphalt type meets the technical requirements of the Chinese specification "Highway Asphalt Pavement Design Specification" (JTG D50-2017).

Table 2. Main technical specifications of 70# base asphalt and SBSMA.

Technical Specifications		70# Base Asphalt	Technical Requirements	SBSMA	Technical Requirements	Testing Methods
Penetration/0.1 mm		69	60~80	48	30~60	T0604
Softening point/°C		48.0	≥46	90	≥60	T0606
Ductility at 15 °C/cm		>100	≥100	——	——	T0605
Ductility at 5 °C/cm		——	——	27	≥20	T0605
Flash point/°C		294	≥260	281	≥260	T0611
Dynamic viscosity at 60 °C/(Pa·s)		195	≥180	——	——	T0620
Rotational viscosity at 135 °C/(Pa·s)		——	——	1.47	≤3	T0620
Density at 15 °C/(g·cm^{-3})		1.018	Measured records	1.030	Measured records	T0603
After TFOT * test (163 °C, 5 h)	Mass change/%	−0.04	±0.8	−0.01	±1.0	T0609
	Penetration ratio/%	65.7	≥61	77	≥65	T0609T0604
	Ductility at 15 °C/cm	10	≥4	——	——	T0609T0605
	Ductility at 5 °C/cm	——	——	17	≥15	T0609T0605

* TFOT refers to the thin film oven test.

3.1.3. Biochar-Modified Asphalt

Based on existing research [22], sludge-based biochar and WWBMA were prepared using a high-speed shear method with a 6% dosage. The preparation process is illustrated in Figure 3.

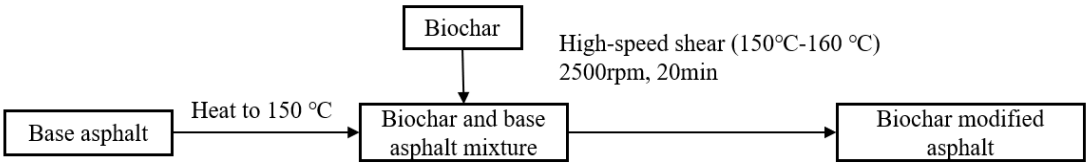

Figure 3. Preparation process of biochar-modified asphalt.

3.2. Test Methods

3.2.1. Fourier Transform Infrared Spectroscopy (FTIR)

The chemical characteristics of biochar were analyzed using an IRAffinity-1S infrared spectrometer. Samples were prepared using the pellet method, in which a certain amount of biochar powder was mixed and ground with KBr powder, then pressed into thin pellets for analysis. The testing wavelength ranged from 400 to 4000 cm^{-1}, with a resolution of 4 cm^{-1}. The FTIR test of each asphalt adopted the attenuated total refraction (ATR) attachment method; the asphalt was heated and dropped on the glass slide and then cooled and placed in the infrared spectrometer for analysis, with a test wavelength of 400 to 4000 cm^{-1} and a resolution of 4 cm^{-1}.

3.2.2. X-Ray Diffraction Analysis (XRD)

The crystalline structure of biochar was analyzed using a Bruker D8 Advance X-ray diffractometer (Germany). Prior to testing, the biochar was thoroughly ground and passed through a 200-mesh sieve. The scanning angle ranged from 5° to 85°, with a scanning rate of 2°/min.

3.2.3. Atomic Force Microscopy Test (AFM)

The asphalt samples were tested using an AFM produced by Bruker Dimension Icon, employing the tapping mode. Prior to this experiment, the asphalt was quickly heated to a molten state in an oven. A suitable amount of the flowing asphalt was then dropped onto a glass slide and placed in a 140 °C oven for 5 min to obtain a smooth surface. After removal, the sample was allowed to cool naturally to room temperature. Since silica (SiO_2) is the main component of aggregates, an RTESPA-150 probe was used in the experiment to simulate the interfacial adhesion characteristics between mineral aggregates and asphalt. The probe had a tip radius of 8 nm, a standard cantilever elastic constant of 6 N/m, a beam length of 125 μm, and a resonance frequency of 150 kHz. The scanning area was 20 μm × 20 μm, with an image resolution of 512 × 512. Based on the AFM scanning results, the analysis of the bee-like structure area ratio and surface roughness of the asphalt was conducted.

1. Bee Area Ratio

The bee-like structure area ratio was calculated using Image-Pro Plus 6.0 software, which measures the percentage of the area occupied by the bee-like structures within the AFM scanning area. Before calculation, the AFM images were binarized to facilitate the extraction of geometric features, making it easier to quantify the characteristics of the bee-like structures;

2. Surface Roughness

Commonly used parameters for describing surface roughness include the average roughness R_a and the root mean square roughness R_q. Generally, both R_a and R_q represent similar surface roughness results, with R_q always being slightly larger than R_a, and R_q being more sensitive when measuring points on the perimeter of the image. Using Nanoscope Analysis software 3.00.0.0 and the Roughness module, the parameters R_a and R_q that characterize surface roughness can be obtained.

3.2.4. Contact Angle Test

The contact angles between asphalt and different testing liquids were measured using a DSA100 contact angle measuring instrument (Germany). The testing liquids included

distilled water, glycerol, and formamide, which have known SFE parameters and do not dissolve or react with asphalt. The testing temperature was set to room temperature at 25 °C. To ensure accuracy, each sample underwent 5 parallel tests, and the results were averaged. Based on the aforementioned SFE theory, the SFE (γ), non-polar dispersion component (γ^{LW}), polar acid-base component (γ^{AB}), polar acid component (γ^{+}), and polar base component (γ^{-}) for different asphalts and aggregates were calculated from the measured contact angles. The SFE parameters of the testing liquids are shown in Table 3, and the contact angle testing process is illustrated in Figure 4.

Table 3. SFE parameters of testing liquids (mJ/m^2).

Testing Liquids	γ_l	γ_l^{LW}	γ_l^{AB}	γ_l^{+}	γ_l^{-}
Distilled water (H_2O)	72.8	21.8	51.0	25.5	25.5
Glycero ($C_3H_8O_3$)	64.0	34.0	30.0	3.92	57.4
Formamide (CH_3NO)	58.0	39.0	19.0	2.28	39.6

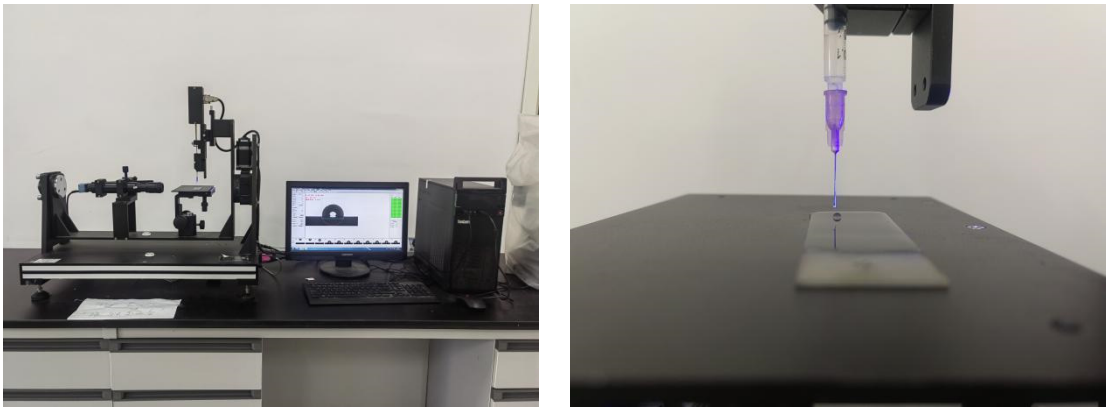

Figure 4. Contact angle test.

The methodological flowchart of this study is shown in Figure 5.

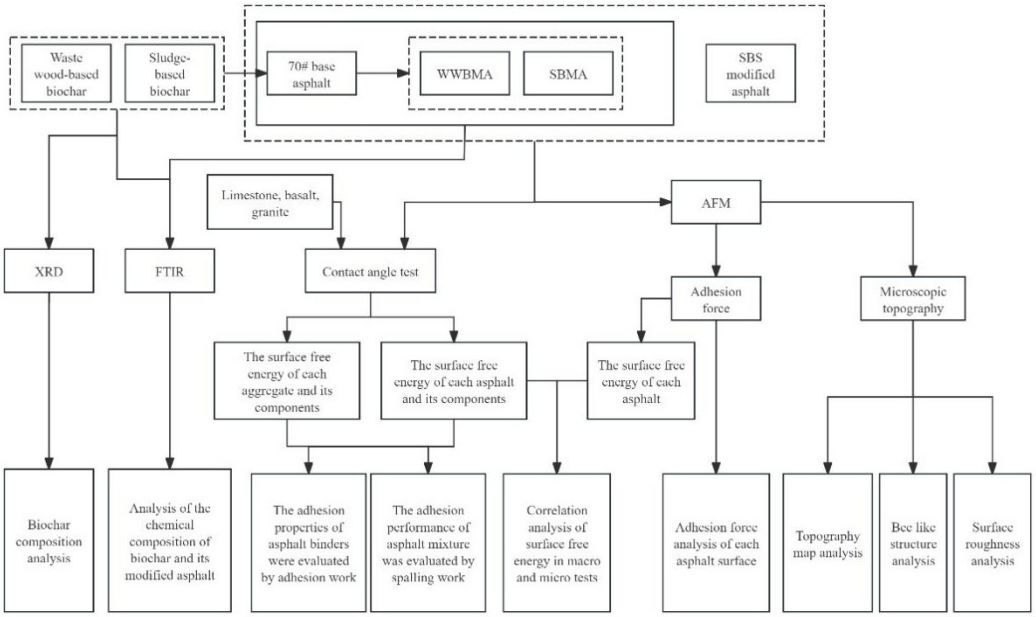

Figure 5. Methodological flowchart of this study.

4. Results and Discussion

4.1. Basic Properties of Biochar

FTIR and XRD were used to analyze the chemical composition and mineral composition of sludge-based biochar and waste wood-based biochar.

4.1.1. FTIR

The FTIR test results of biochars and their modified asphalts are shown in Figure 6.

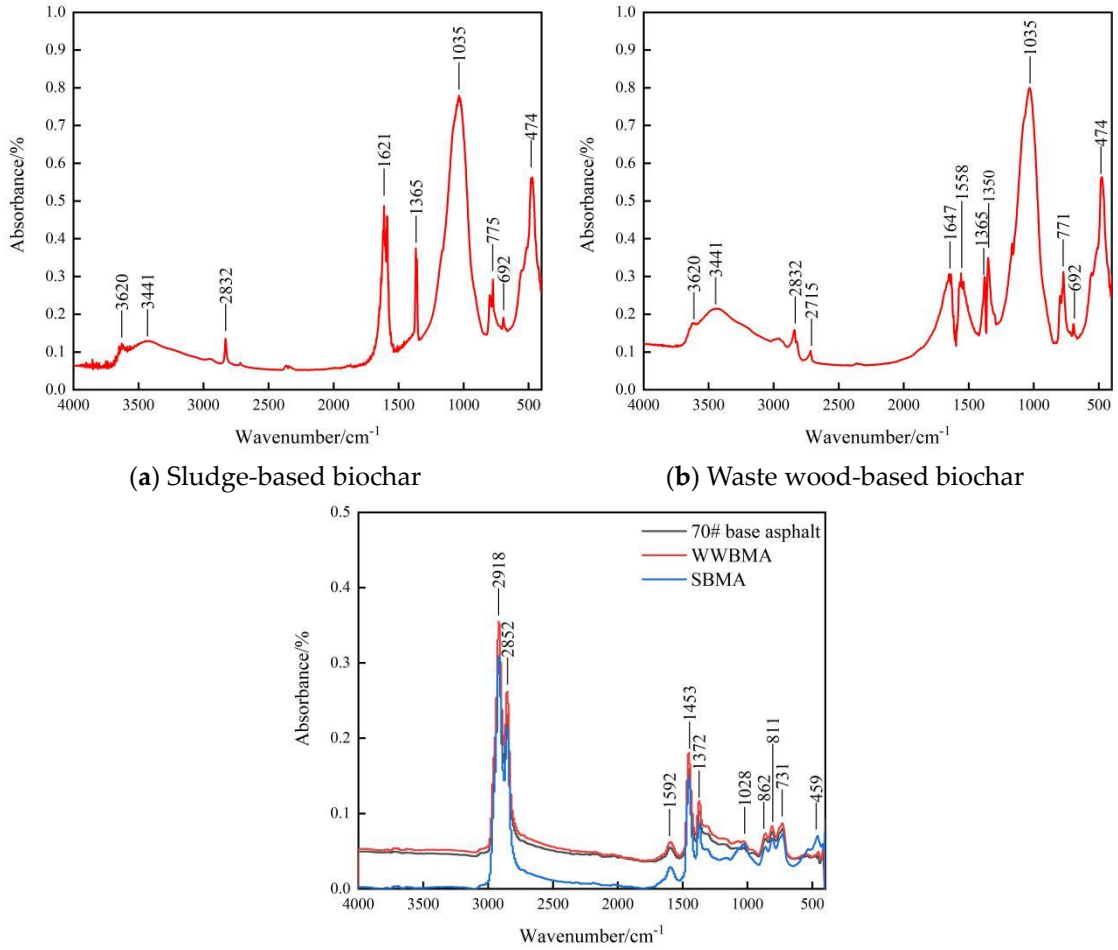

(**a**) Sludge-based biochar (**b**) Waste wood-based biochar

(**c**) 70# base asphalt and biochar-modified asphalts

Figure 6. FTIR test results of biochars and their modified asphalts.

Previous studies have shown [23] that the chemical functional groups of saturated alkanes mainly included C-H vibrations and C-C skeletal vibrations. The C-H vibrations consist of C-H stretching vibrations (in the range of 3000 to 2830 cm^{-1}) and C-H bending vibrations (near 1460 cm^{-1} and 1350 cm^{-1}), while the C-C skeletal vibrations occur in the range of 1100 to 1020 cm^{-1}. The C=C stretching vibrations primarily occur in the range of 1700 to 1370 cm^{-1}, and the C=C stretching vibrations of the aromatic ring mainly occur in the range of 1610 to 1370 cm^{-1}.

Figure 6a,b show that both biochar samples exhibit significant absorption peaks for C-H vibrations and C-C skeletal vibrations of saturated alkanes at 2832 cm^{-1}, 1365 cm^{-1}, and 1035 cm^{-1}, as well as C=C stretching vibration absorption peaks of the aromatic ring at 1621 cm^{-1} or 1647 cm^{-1}. The C-H bending vibration absorption peaks of olefin or aromatic at 775 cm^{-1} and 692 cm^{-1}, and the C-H expansion vibration absorption peaks of alkane at 474 cm^{-1}. The waste wood-based biochar shows a distinct aromatic C=C stretching vibration absorption peak at 1558 cm^{-1}, which is different from that of the

sludge-based biochar. This indicates that the chemical composition of biochar primarily consists of saturated alkanes and unsaturated carbon chain groups, with the waste wood-based biochar also containing phenolic groups. The functional groups on the surface of biochar can form chemical adsorption with asphalt, and the methyl and carbon chain organic compounds contained in the biochar are readily soluble in asphalt, allowing for strong physical adsorption with the polar molecules in asphalt [24]. This facilitates a thorough integration with asphalt, enhancing adhesion performance.

Figure 6c shows the FTIR test results of 70# base asphalt, WWBMA, and SBMA; the results show that there is no significant difference between WWBMA and 70# base asphalt, and a new vibration absorption peak representing C-C saturated alkanes appears at 1028 cm^{-1} in SBMA, which indicates that sludge-based biochar can produce chemical interaction with base asphalt, while there is only physical interaction between waste wood-based biochar and base asphalt.

4.1.2. XRD

The XRD test results for each asphalt type are shown in Figure 7.

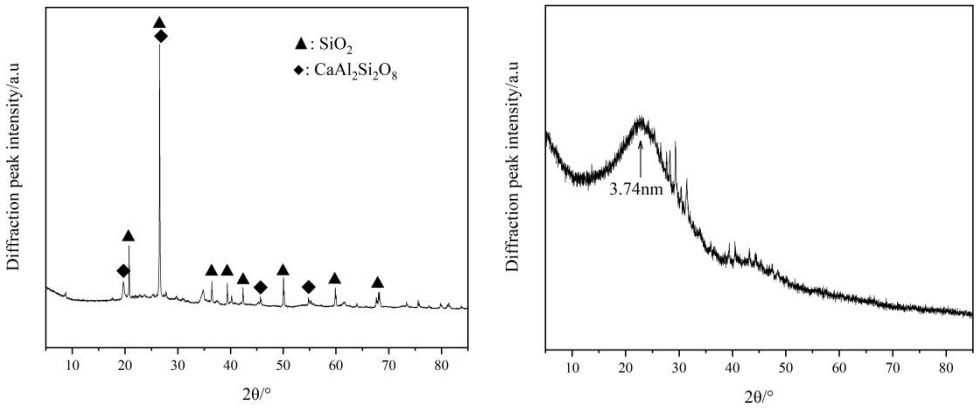

(**a**) Sludge-based biochar (**b**) Waste wood-based biochar

Figure 7. XRD test results for each asphalt type.

As shown in Figure 7, the test results for sludge-based biochar and waste wood-based biochar differ significantly. The sludge-based biochar exhibits distinct crystal diffraction peaks due to the presence of a larger number of crystals, primarily composed of quartz (SiO_2) and feldspar ($CaAl_2Si_2O_8$). In contrast, the waste wood-based biochar does not show sharp diffraction peaks but presents broad and gentle scattering peaks in the range of 2θ from 15° to 36°. This corresponds to the d_{002} diffraction peak of crystalline carbon fibers, which is formed by the carbonization of cellulose and hemicellulose in waste wood, resulting in a graphitized structure [25].

4.2. Microstructural Analysis of Biochar-Modified Asphalt

4.2.1. Morphological Analysis

The 2D and 3D AFM morphology images of base asphalt, SBSMA, and biochar-modified asphalt at room temperature are shown in Figure 8. It is evident from Figure 8 that each type of asphalt exhibits a distinct two-phase structure at the microscopic scale, consisting of bee-like structures (Beephase) and a continuous phase (Perpetua-phase). The bee-like structures appear as alternating black and white stripes in the 2D morphology image, while in the corresponding 3D morphology image, the peaks are bright white protrusions, and the valleys are dark recesses in the opposite direction. Regarding the formation of the bee-like structures, Loeber [26] suggested that it is due to the aggregation effect of asphaltenes on the surface, a conclusion that has been supported by researchers such as Wu et al. [7]. On the other hand, Yang [23] posited that the bee-like structures on the asphalt surface are crystalline formations resulting from the co-crystallization of wax

and large macromolecules such as asphalt. Pauli [10] similarly believed that the primary component of the bee-like structures is wax crystals, formed by the strong polarity of asphaltenes and high molecular waxes that bind a portion of the colloid dispersed in the oil phase.

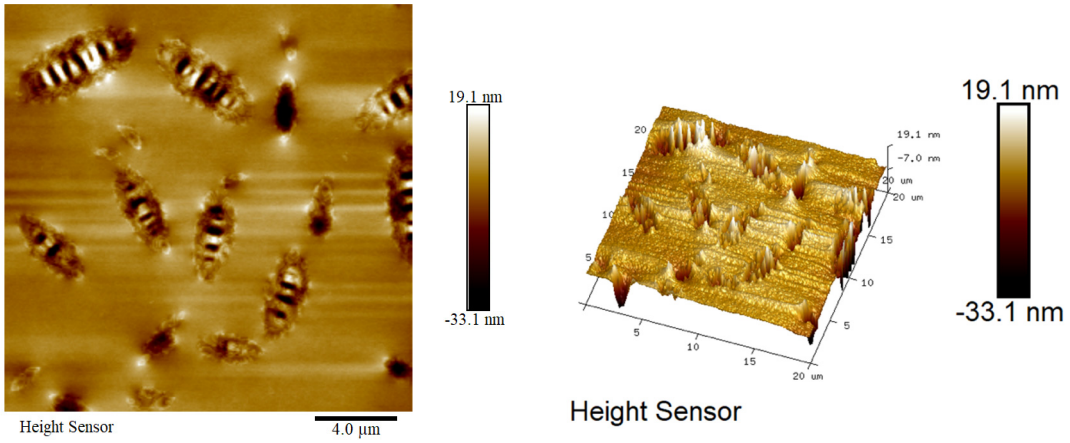

(**a**) 70# base asphalt

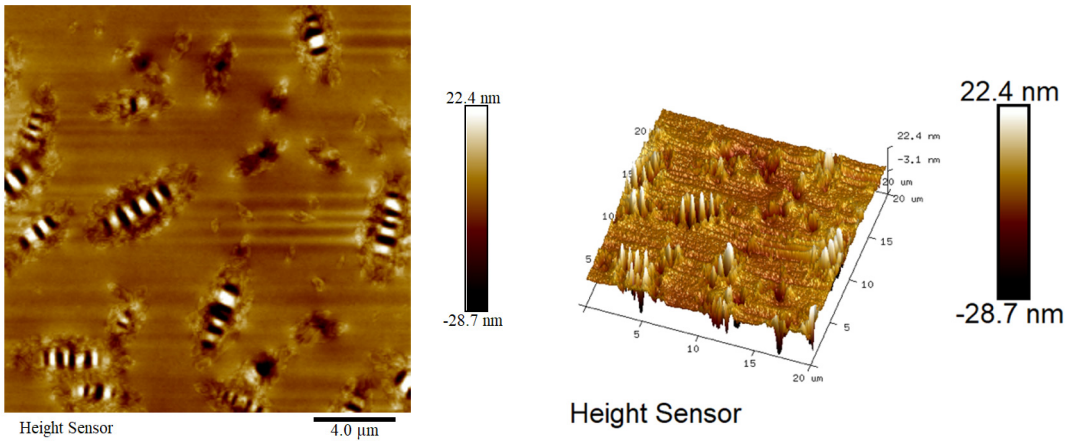

(**b**) SBSMA

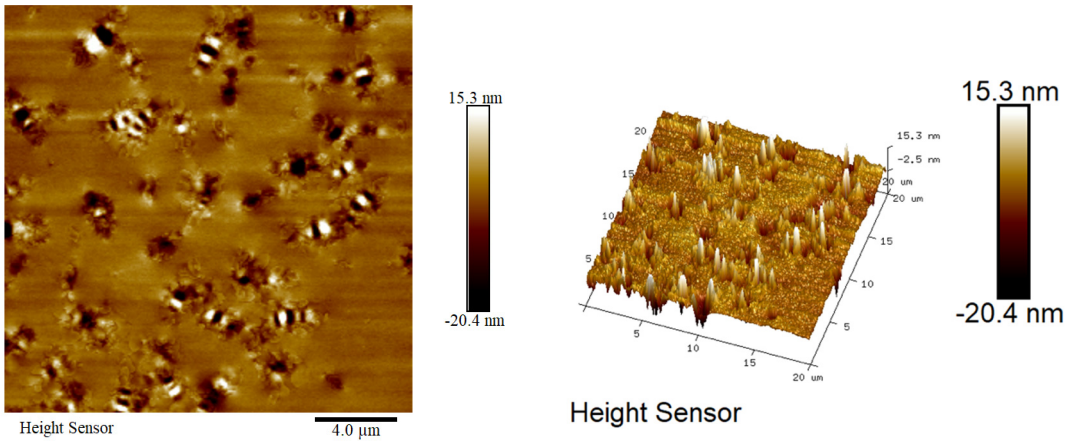

(**c**) SBMA

Figure 8. *Cont.*

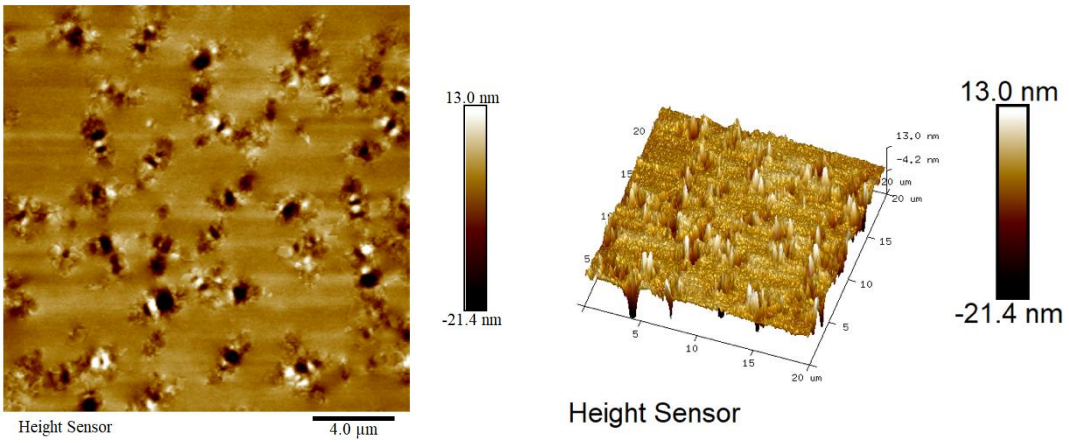

(**d**) WWBMA

Figure 8. The 2D and 3D morphology images of each asphalt sample from AFM.

From the 2D morphology images of each asphalt type in Figure 8, it can be observed that the number of bee-like structures in sludge-based biochar (SBMA) and WWBMA (Figure 8c,d) is significantly higher than that in 70# base asphalt (Figure 8a). Additionally, the bee-like structures in the biochar-modified asphalt are smaller in size and more uniformly distributed. This indicates that biochar can greatly increase the number of bee-like structures on the microscopic surface of asphalt while significantly reducing the area of individual bee-like structures. From the 3D morphology images of each asphalt type in Figure 8, it is evident that the surface of biochar-modified asphalt contains more needle-like crystals compared to base asphalt, with a relatively lower height and a more uniform distribution of needle-like crystals. This suggests that biochar can alter the distribution of the crystalline structure on the surface of asphalt, thereby enhancing its stability.

4.2.2. Bee Structure Area Ratio

To quantitatively analyze the impact of biochar on the adhesion properties of asphalt, the bee-like structure area ratio was calculated using Image-Pro Plus software. Before the calculation, the AFM images were binarized to facilitate the extraction of geometric features for a more intuitive calculation of the characteristics of the bee-like structures. A typical result of the binarization process is shown in Figure 9.

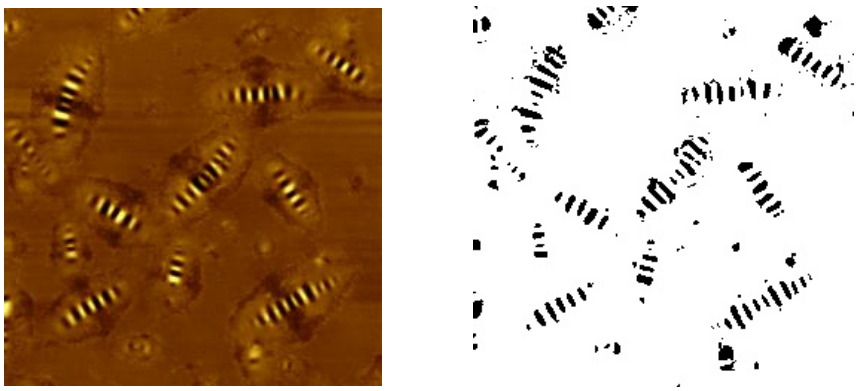

Figure 9. Binarization results of AFM morphology.

By analyzing the binarized images, the number of bee-like structures, average area, and area ratio for each asphalt type were obtained, as shown in Figure 10.

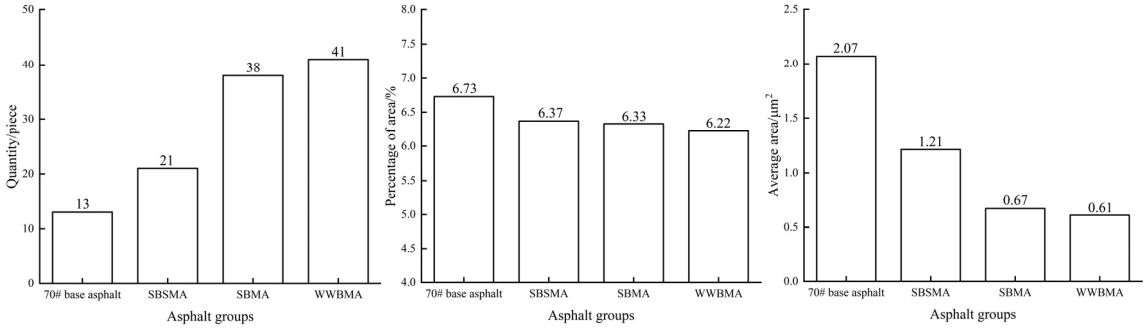

(**a**) Quantity (**b**) Area ratio (**c**) Average area

Figure 10. Characteristics of bee-like structures in each asphalt type.

The changes in the characteristics of the bee-like structures indicate that biochar has a significant impact on the microstructure of asphalt. Compared to 70# base asphalt, the number of bee-like structures in sludge-based biochar and WWBMA increased by 192% and 215%, respectively, while the area ratios decreased by 5.9% and 7.6%. The average areas decreased by 67.6% and 70.5%, respectively. Biochar significantly increases the number of bee-like structures on the microscopic surface of asphalt while reducing the area of individual bee-like structures, which is consistent with the morphological analysis results. This may be due to the rich porous structure of biochar, which forms a stable structure within the asphalt matrix, restricting the movement and aggregation of asphalt molecules. As the temperature decreases, the molecules do not have enough time to relax to lower energy positions, leading to phase changes in a small range, which is manifested as a reduction in the area of the bee-like structures and an increase in the number of smaller bee-like structures [27].

4.2.3. Surface Roughness

The surface roughness of each asphalt type was determined using the "Roughness" module in the AFM analysis software Nano Scope Analysis 3.00.0.0 to study the evolution of the microstructure of modified asphalt at the nanoscale. The larger the surface roughness of the asphalt, the better the contact between the asphalt and the aggregate. Figure 11 shows the calculated results of Rq and Ra values for the micro surfaces of each asphalt type.

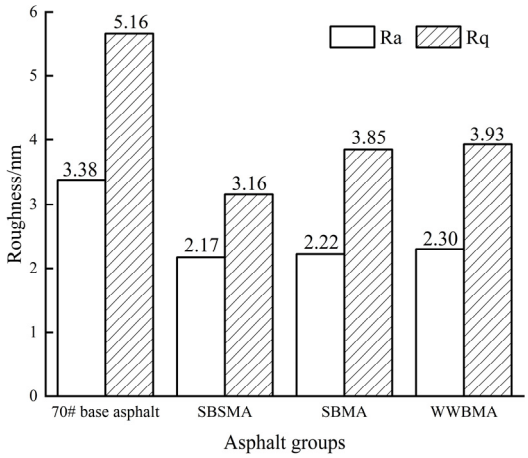

Figure 11. Calculation results of micro surface roughness for each asphalt type.

From Figure 11, it can be seen that both the Ra and Rq values of BMA are higher than those of the matrix asphalt. Compared to the 70# base asphalt, the Ra values of the SBMA and WWBMA increased by 8.82% and 12.75%, respectively, while the Rq values increased by 24.37% and 21.84%. This indicates that biochar significantly increases the

surface roughness of asphalt; with the increase in asphalt surface roughness, mechanical occlusion between asphalt and aggregate is more likely to occur, which improves the adhesion of asphalt.

4.3. Micro-Adhesion Performance Analysis of BMA

4.3.1. Adhesion Force of Asphalt Based on AFM Testing

The AFM-QNM mode was used to test the microscopic mechanical properties of each asphalt sample at room temperature. The adhesion force obtained from the experiments is an important parameter for evaluating the adhesion performance of asphalt, providing a reference for assessing the water damage resistance of asphalt mixtures at a macro level. The adhesion force test results for each asphalt sample are presented in Figure 12.

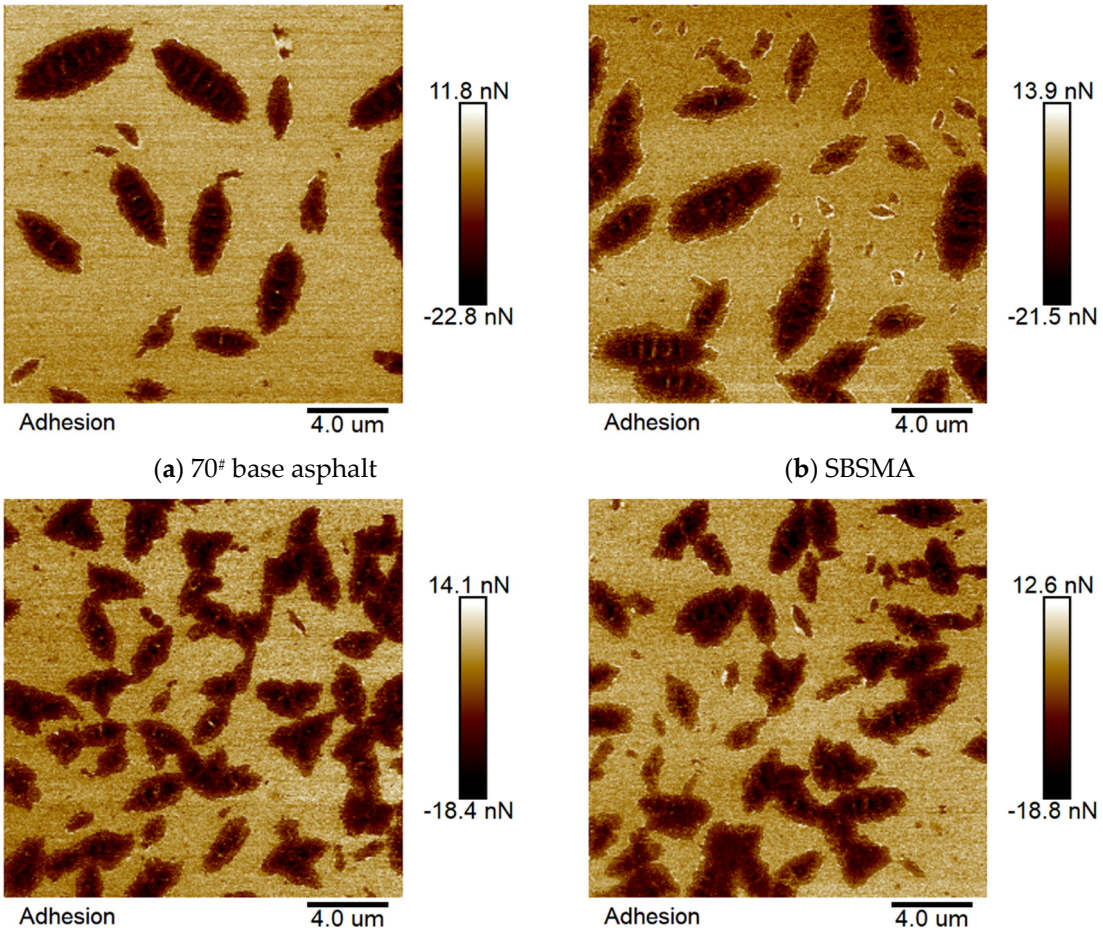

(**a**) 70# base asphalt (**b**) SBSMA

(**c**) WWBMA (**d**) SBMA

Figure 12. Adhesion force test results for each asphalt sample.

From Figure 12, it can be observed that the adhesion force test results are similar to the morphological results, both exhibiting two phases: Beephase and Perpetua-phase.

There is a significant difference in adhesion force between these phases, with the color of the images transitioning from dark to light representing an increase in adhesion force. The color differences indicate that the bee structure is in a low-adhesion phase, while the non-bee structure is in a high-adhesion phase. This is attributed to the fact that the non-bee structure primarily consists of lower molecular weight saturated and aromatic compounds, whereas the bee structure is mainly composed of high molecular weight asphaltenes and wax crystals, resulting in relatively lower adhesion forces.

To further quantify the adhesion force metrics of each asphalt sample, the data from Figure 11 were extracted and analyzed using Origin 9.5 software, as shown in Figure 13.

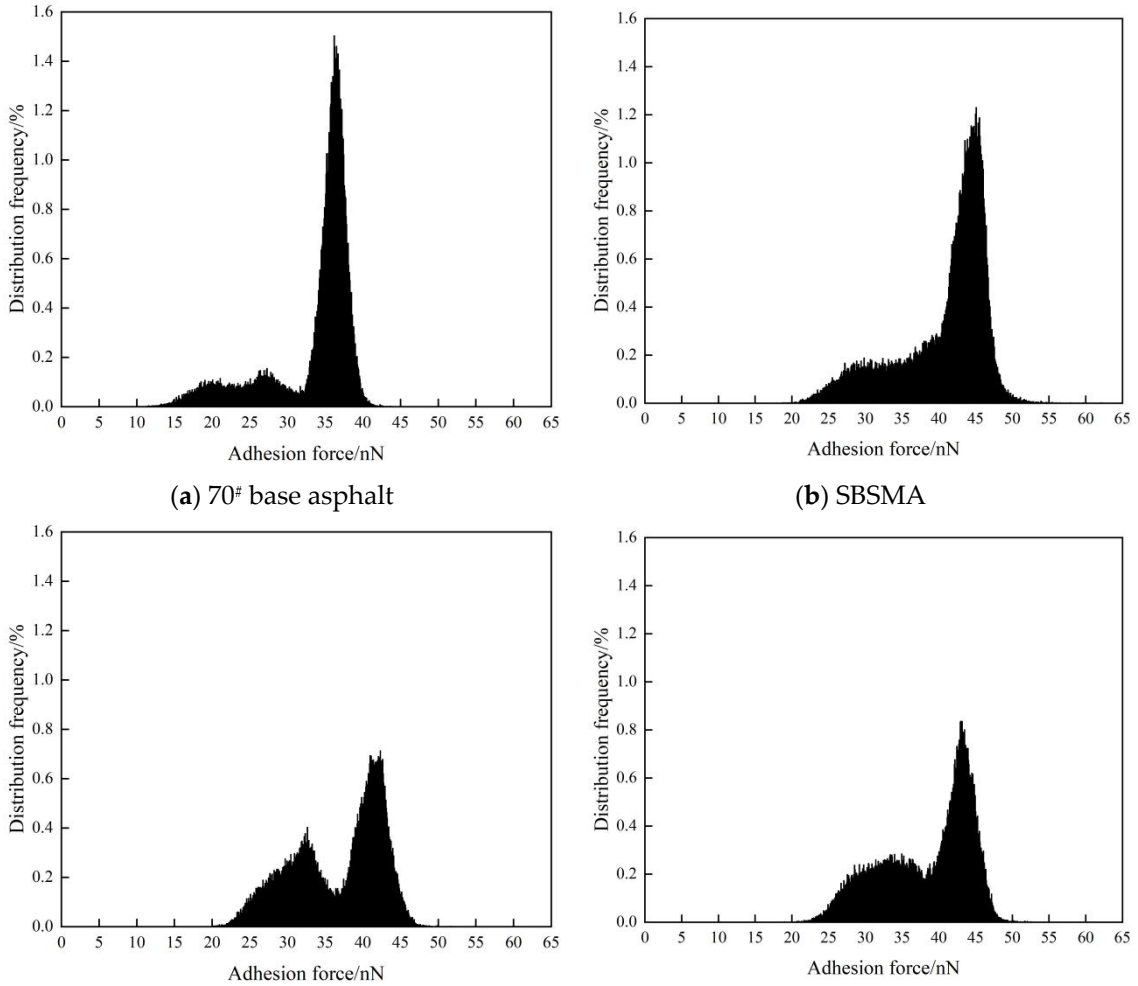

Figure 13. Histogram of adhesion force data distribution for each asphalt sample.

From Figure 13, it can be seen that the adhesion force data for the asphalt samples exhibit a concentrated distribution pattern. The addition of biochar effectively improved the overly concentrated adhesion force distribution of the matrix asphalt, reducing the difference in adhesion force between the bee structure and non-bee structure regions, thus minimizing stress concentration at the microscopic level. By selecting the average value of the adhesion force data as a representative value for overall adhesion, the analysis results for each asphalt's adhesion force are shown in Table 4. It can be observed from Table 4 that compared to the 70# base asphalt, the adhesion forces of the SBMA and WWBMA increased by 14.28% and 9.25%, respectively, indicating that the biochar modifier enhanced the adhesion performance of the asphalt. This improvement is attributed to the rough surface and rich pore structure of biochar, which increases the adsorption sites on the surface and enhances the surface charge capacity, thereby improving the bonding ability of biochar with asphalt and benefiting the adhesion characteristics of the asphalt.

Table 4. Representative values of overall adhesion strength for different asphalts.

Types of Asphalt	70# Base Asphalt	SBSMA	WWBMA	SBMA
Adhesion strength/nN	33.61	40.80	36.72	38.41

Combined with the test results of the adhesion of each asphalt in Figure 12, the adhesion distribution of each asphalt in Figure 13, and the representative values of the

overall adhesion of each asphalt in Table 4, the microscopic mechanism of biochar to improve the adhesion performance of asphalt can be proposed. Biochar can improve the adhesion of asphalt by improving the adhesion between the continuous phase and the bee-like structure on the asphalt surface, reducing the area of the bee-like structures, increasing the number of bee-like structures, and improving the surface roughness of the asphalt. This is due to the rich pore structure of biochar materials, which allows the asphalt not only to adsorb on the surface of biochar but also enter the internal pores of biochar and limit the movement and aggregation of asphalt molecules, increasing the content of structural asphalt. Compared with free asphalt, structural asphalt has more stable properties and stronger adhesion.

4.3.2. Asphalt SFE Based on AFM Testing

With the application and development of contact mechanics in AFM testing, the Derjaguin–Muller–Toporov (DMT) and Johnson–Kendall–Roberts (JKR) models in this field can effectively simulate the contact between the probe and the asphalt surface while considering the SFE resulting from the interaction between two objects [28]. The DMT theory assumes the presence of adhesive forces on the surface but only considers the contact area and the surrounding regions, neglecting the influence of forces within the contact area, which leads to an underestimation of the force magnitude in the contact region. This theory is applicable to systems with small radii of curvature, low adhesion energy, and high elastic modulus. On the other hand, the JKR theory allows for local deformation but only applies to the contact area, neglecting the effects of forces outside the contact region, thereby underestimating the external load effects. This theory is suitable for systems with large radii of curvature, high adhesion energy, and low elastic modulus [29]. In this study, the JKR model is selected as the contact mechanics calculation model for asphalt adhesion work and SFE. Based on this model, the relationship between adhesion force and adhesion work is derived, as shown in Equation (9):

$$F_{ab} = \frac{3}{2}\pi RW \tag{9}$$

In the equation, F_{ab} is the adhesion force (nN); R is the contact radius (m), and W is the adhesion energy (mJ/m^2).

The JKR model facilitates the transition from adhesion force to adhesion work. Based on the principle of work–energy conversion, the Fowkes model can be used to transform adhesion work into SFE [30], with the conversion relationships illustrated in Equations (10) and (11):

$$\gamma_{ab} = \gamma_a + \gamma_b - 2\sqrt{\gamma_a^d \gamma_b^d} \tag{10}$$

$$W_{ab} = 2\sqrt{\gamma_a^d \gamma_b^d} \tag{11}$$

In the equations, γ_{ab} represents the SFE between the materials (mJ/m^2); γ_a and γ_b represent the surface free energies of the two materials (mJ/m^2), and W_{ab} represents the adhesion work between the materials (mJ/m^2).

As a material composed of non-polar hydrocarbons, asphalt has a SFE component dominated by the dispersive component, allowing $\gamma_a \approx \gamma_b$ for approximate calculations [30]. With the SFE of the probe γ_b known, and by considering the adhesion work between the probe and the asphalt surface, the SFE of asphalt γ_a can be calculated. The results for asphalt adhesion work and SFE calculations are shown in Table 5.

From Table 5, it can be observed that the addition of biochar modifiers enhances the adhesion work and SFE of asphalt. During the process of forming a mixture system through the contact between asphalt and aggregates, a greater change in SFE indicates that more energy is released from the system, resulting in a more stable asphalt–aggregate system. Compared to 70# base asphalt, the SFE of SBMA and WWBMA increased by 30.60% and 19.36%, respectively, achieving 88.63% and 81.00% of the SFE of SBSMA.

Table 5. Adhesion work and SFE calculated based on AFM adhesion force.

Asphalt Type	Adhesion Force/nN	Adhesion Work/(mJ/m^2)	SFE/(mJ/m^2)
70$^{\#}$ base asphalt	33.61	445.77	24.84
SBSMA	40.80	541.13	36.60
WWBMA	36.72	487.01	29.65
SBMA	38.41	509.43	32.44

4.3.3. Correlation Analysis of Macro/Micro SFE of Asphalt

Adhesion force can be used to characterize the mechanical behavior of biochar-modified asphalt, and based on this, adhesion work and SFE can be further calculated using relevant models. To evaluate the correlation of mechanical indicators at the macro and micro scales, a Pearson correlation analysis was conducted between the SFE obtained from AFM testing and calculations and the SFE obtained from contact angle measurements at the macro scale using the same experimental materials. Pearson correlation analysis can be used to measure the degree of linear correlation between two variables, with the strength of the linear correlation described by the correlation coefficient r. A larger absolute value of r indicates a stronger correlation between the two variables.

The average contact angle test results of three testing liquids on the asphalt surface are shown in Table 6.

Table 6. Contact angle test results on asphalt surface (unit: °).

Types of Asphalt	70$^{\#}$ Base Asphalt	SBSMA	WWBMA	SBMA
Distilled Water	97.52	103.30	100.65	102.59
Glycerol	87.36	89.98	88.98	89.43
Formamide	80.43	78.17	79.06	78.59

As can be seen from Table 6, compared to 70# base asphalt, biochar increases the contact angle between the testing liquids and the modified asphalt, thereby enhancing the hydrophobicity of the asphalt. The contact angle values between the testing liquids and the asphalt binder are larger than those with the aggregate because asphalt is a non-polar material with strong hydrophobicity, whereas aggregate, being a mineral, is hydrophilic. This makes the testing liquids more likely to spread and distribute on the aggregate surface, resulting in relatively smaller contact angle values. By substituting the test data from Table 6 into Equations (1) and (6), the SFE of the asphalt and its components can be obtained, as shown in Table 7.

Table 7. SFE of asphalt and its components (unit: mJ/m^2).

Types of Asphalt	70$^{\#}$ Base Asphalt	SBSMA	WWBMA	SBMA
γ_s	24.94	36.73	29.54	32.81
γ^{LW}	24.46	36.15	29.29	32.43
γ_S^{AB}	0.48	0.58	0.25	0.38
γ_S^+	2.07	0.29	1.00	0.44
γ_S^-	0.03	0.28	0.02	0.08

From the data in Table 7, it can be seen that compared to 70# base asphalt, the SFE of SBMA and WWBMA increased by 31.59% and 18.47%, respectively, reaching 89.34% and 80.43% of the SFE of SBSMA.

Using the Pearson correlation coefficient [31], the SFE from the AFM micro-experiments and the SFE from the contact angle macro-experiments for each type of asphalt in Tables 5 and 7 were analyzed as sample data.

Calculations show that the correlation coefficient (r) between micro SFE and macro SFE is 0.9993, indicating a very strong correlation and suggesting that the micro-mechanical

indicators of asphalt exhibit consistent variation with the macro-mechanical indicators. Notably, the JKR model was used to calculate micro SFE, which neglects polar components and approximates the SFE of asphalt as equal to its dispersive component. In contrast, the macro-experiments utilized contact angle measurements to account for both dispersive and polar components, resulting in macro SFE values being greater than micro SFE.

Comparing the data for macro and micro SFE reveals that they can mutually validate each other. While AFM experiments cannot derive data for the polar component of SFE, they can explore the surface structural characteristics of asphalt at a microscopic level through micromorphology and adhesion force metrics, thereby evaluating asphalt's adhesive performance. Conversely, contact angle experiments provide data on SFE and its components, allowing for a multifaceted characterization of asphalt adhesion differences. Additionally, contact angle testing equipment is relatively low-cost and simple to operate, though results may have larger errors. Therefore, both AFM and contact angle tests have their advantages and disadvantages; it is recommended to combine results from both methods for a comprehensive evaluation of asphalt's adhesive performance, as they can complement and corroborate each other.

4.4. Analysis of Macroscopic Adhesion of Biochar-Modified Asphalt

(1) SFE and Its Components

From the data in Table 7, it can be seen that the addition of biochar increases the SFE of asphalt, a conclusion consistent with the AFM test results. Moreover, the dispersive component of each asphalt's SFE is significantly greater than the polar component. The dispersive component primarily includes Lonson dispersive force, Debye induction force, and Keesom orientation force [32], all of which belong to the physical adhesion of adhesive work. A larger dispersive component indicates stronger physical adhesion. Compared to 70# base asphalt, the dispersive components of SBMA and WWBMA increased by 32.61% and 19.75%, respectively. On the other hand, the polar component mainly includes Lewis acid-base interactions [33]; a larger polar component makes it easier for moisture to be adsorbed, leading to easier peeling of asphalt from aggregates. Compared to 70# asphalt, the polar components of SBMA and WWBMA decreased by 20.09% and 47.01%, respectively. In summary, the addition of biochar increases the dispersive component and decreases the polar component of asphalt, making it more difficult for moisture to be adsorbed on the asphalt surface and enhancing its water stability. The increase in the dispersive component may be due to the abundant pores and carbon chain structure of biochar enhancing the van der Waals forces when combined with asphalt. Additionally, the acidic component of each asphalt is greater than the basic component, indicating better bonding performance of asphalt with basic aggregates, which aligns with existing conclusions;

(2) Adhesion Work and Peel Work

By substituting the SFE and its components of asphalt and aggregates into Equations (6) and (8), we can obtain adhesion work and peel work, which quantitatively evaluate the adhesive performance between asphalt and aggregates. Adhesion work refers to the energy released when asphalt and aggregates combine from two interfacial systems into one interfacial system under anhydrous conditions. The greater the adhesion work, the more energy is released during the formation of the asphalt–aggregate system, leading to greater stability of the entire system. Peel work refers to the energy released when water molecules enter the asphalt–aggregate interface to form a three-phase interfacial system; the greater the peel work, the more easily water molecules can replace the adhesion between asphalt and aggregates, making the bond weaker and increasing the likelihood of moisture-related damage due to poor water stability in the mixture.

The SFE and its components of the aggregates can be obtained similarly to asphalt, with the contact angle test results for three testing liquids on the dry, smooth aggregate surface shown in Table 8.

Table 8. Contact angle test results of aggregate surface (unit: °).

Aggregate Type	Granite	Limestone	Basalt
Distilled water	69.5	70.6	73.3
Glycerol	58.1	54.8	59.5
Formamide	45.6	37.4	44.2

By substituting the data from Table 8 into Equations (1) and (6), the SFE of the aggregates and their components are obtained, as shown in Table 9.

Table 9. SFE of aggregate and its components (unit: mJ/m^2).

Aggregate Type	Granite	Limestone	Basalt
γ_S	46.10	57.54	52.46
γ^{LW}	42.49	56.59	51.74
γ_S^{AB}	3.61	0.95	0.72
γ_S^+	9.25	5.65	5.86
γ_S^-	0.35	0.04	0.02

Substituting the SFE data of asphalt and aggregates from Tables 7 and 9 into Equations (6) and (8), the adhesion work and debonding work between asphalt and each aggregate are obtained, as shown in Table 10.

Table 10. Adhesion work and debonding work between asphalt and each aggregate (unit: mJ/m^2).

Types of Asphalt		70# Base Asphalt	SBSMA	SBMA	WWBMA
W_{as}	Granite	67.19	82.31	76.79	72.51
	Limestone	75.77	93.25	87.32	82.42
	Basalt	72.38	89.28	83.53	78.77
$W_{a\omega s}$	Granite	−55.55	−67.26	−64.57	−60.57
	Limestone	−64.09	−78.38	−75.51	−70.85
	Basalt	−63.71	−77.56	−74.82	−70.25

As shown in Table 9, significant differences were observed in SFE and its components among different aggregates. Limestone exhibited the highest SFE, followed by basalt, with granite having the lowest. The dispersive component of different aggregates was much larger than the polar component, and their relative magnitudes were consistent with the SFE. Granite had the largest polar component, with its acidic component being particularly prominent, indicating that, compared to limestone and basalt, granite was more prone to bonding with water molecules, while its bonding ability with asphalt was relatively weaker. This conclusion is consistent with existing research findings [34].

From Table 10, it can be seen that the addition of biochar effectively enhances the adhesion performance between asphalt and aggregates. In the asphalt–limestone system, compared to the 70# base asphalt, the incorporation of SBMA and WWBMA increases the adhesion work by 15.25% and 8.78%, respectively, achieving 93.65% and 88.39% of the SBSMA's adhesion work. The debonding work decreases by 17.82% and 10.55%, corresponding to 96.33% and 90.39% of the SBSMA's debonding work.

The adhesion performance of the asphalt–basalt system was similar to that of the asphalt–limestone system, while the adhesion performance of the asphalt–granite system was weaker than that of the asphalt–limestone system. In the asphalt–granite system, compared to 70# base asphalt, the addition of SBMA and waste WWBMA increased the adhesion work by 14.28% and 7.91%, respectively, reaching 93.30% and 88.10% of that of SBSMA. Meanwhile, the stripping work was reduced by 16.23% and 9.05%, respectively, reaching 95.99% and 90.05% of the stripping work of SBSMA.

These results indicate that biochar materials can effectively enhance the adhesion performance between asphalt and aggregates, reduce the moisture sensitivity of asphalt mixtures, and improve the water-stripping resistance of the asphalt film. The effect of sludge-based biochar on enhancing adhesion performance is superior to that of waste wood-based biochar. The main reason may be that the rich carbon chain structure and mineral components in sludge-based biochar undergo physicochemical reactions with asphalt, forming a more stable and dense layered structure. These structures enhance the cohesion and adhesion of asphalt, thereby improving the stripping resistance between asphalt and aggregates.

5. Conclusions

This study analyzed the macro- and micro-adhesion properties of 70# base asphalt, SBSMA, SBMA, and WWBMA to assess the impact of biochar on the adhesion performance of asphalt binders. AFM was used to examine the surface morphology and microstructure of different asphalt binders. SFE was determined through contact angle experiments and SFE theory, allowing for an analysis of the differences in adhesion performance characterized by various testing methods. The following main findings were obtained:

(1) Biochar can improve the formation of bee-like structures on the surface of asphalt, increase the number of bee-like structures, significantly reduce the average area, and be evenly distributed on the asphalt surface, and the surface roughness of asphalt can increase accordingly, which can effectively improve the adhesion of asphalt;

(2) The adhesion force in the bee-like structure regions on the asphalt surface is lower than in the non-bee-like structure regions. The addition of biochar effectively mitigates the excessive concentration of adhesion force on the surface of matrix asphalt, reducing the difference in adhesion force between the bee-like structure regions and the non-bee-like structure regions. This reduces stress concentration at the microscopic level. Additionally, biochar enhances the overall surface adhesion force of the asphalt, further improving the adhesion performance of the asphalt binder;

(3) The SFE obtained from the contact angle test and AFM test are linearly correlated. AFM is suitable for characterizing asphalt adhesion performance at the microscopic level through adhesion force, while the contact angle test is more applicable at the macroscopic level for characterizing the adhesion performance between asphalt and aggregates through adhesion work and debonding work. Both methods provide consistent results in representing asphalt adhesion performance;

(4) Biochar significantly increases the SFE of asphalt and its components, enhances the adhesion work between asphalt and aggregate, and reduces the debonding work, thereby improving the bonding performance between asphalt and aggregate and enhancing the moisture damage resistance of asphalt mixtures. The adhesion between asphalt and aggregates is closely related to the properties of the aggregates, with the asphalt–limestone system demonstrating the best adhesion performance;

(5) The improvement effect of sludge-based biochar on asphalt adhesion performance is better than that of waste wood-based biochar, and the high-value and clean utilization of sludge-based biochar is conducive to the treatment of urban sewage sludge and garbage with huge output, which has significant ecological and environmental benefits. In addition, the raw material cost of sludge-based biochar is lower, and its modified asphalt binder has better economic benefits. Therefore, the comprehensive properties of sludge-based biochar-modified asphalt can be further studied in the future, and the application of solid engineering can be realized as soon as possible.

Author Contributions: Methodology, L.X.; Formal analysis, X.C.; Investigation, W.L.; Resources, Y.L.; Data curation, K.L.; Writing—original draft, Q.L.; Writing—review & editing, H.W. and K.L. All authors have read and agreed to the published version of the manuscript.

Funding: This work was supported by the Key Research and Development Program of Hunan Province, China [Grant No. 2023SK2078].

Institutional Review Board Statement: Not applicable.

Informed Consent Statement: Not applicable.

Data Availability Statement: Data is contained within the article.

Conflicts of Interest: Author Xing Chen was employed by Hunan Expressway Engineering Consulting Co., Ltd. The remaining authors declare that the research was conducted in the absence of any commercial or financial relationships that could be construed as a potential conflict of interest.

Nomenclature

Abbreviation	
SFE	Surface free energy
AFM	Atomic force microscopy
AFM-QNM	AFM-quantitative nano-mechanics
DMT	Derjaguin–Muller–Toporov
JKR	Johnson–Kendall–Roberts
SBSMA	SBS-modified asphalt
BMA	Biochar-modified asphalt
SBMA	Sludge-based biochar-modified asphalt
WWBMA	Waste wood-based biochar-modified asphalt
DSC	Differential scanning calorimetry
FTIR	Fourier transform infrared spectroscopy
XRD	X-ray diffraction analysis

Variables	
γ	Surface free energy
γ_{LW}	Non-polar dispersion component
γ_{AB}	Polar acid-base component
$\gamma+$	Polar acid component
$\gamma-$	Polar base component
W_{as}	Adhesion work
$W_{a\omega s}$	Peel work

References

1. Xing, L.; Xiujuan, H.; Fengde, T. Analysis of sludge generation, treatment, disposal status, and economic trends in typical cities of china. *Environ. Prot. Circ. Econ.* **2021**, *41*, 88–93. [CrossRef]
2. Li-ping, B.; Hongtao, Q.; Ya-ping, F.; Ping, L. Nutrient contents and heavy metal pollutions in composted sewage sludge from different municipal wastewater treatment plants in beijing region. *Environ. Sci.* **2014**, *35*, 4648–4654. [CrossRef]
3. Zhao, S.; Huang, B.; Ye, P. Laboratory evaluation of asphalt cement and mixture modified by bio-char produced through fast pyrolysis. In *Pavement Materials, Structures, and Performance*; ASCE: Reston, VA, USA, 2014; pp. 140–149.
4. Zhang, R.; Wang, H.; Ji, J.; Wang, H. Viscoelastic properties, rutting resistance, and fatigue resistance of waste wood-based biochar-modified asphalt. *Coatings* **2022**, *12*, 89. [CrossRef]
5. Walters, R.; Begum, S.A.; Fini, E.H.; Abu-Lebdeh, T.M. Investigating bio-char as flow modifier and water treatment agent for sustainable pavement design. *Am. J. Eng. Appl.* **2015**, *8*, 138–146. [CrossRef]
6. Jäger, A.; Lackner, R.; Eisenmenger-Sittner, C.; Blab, R. Identification of four material phases in bitumen by atomic force microscopy. *Road Mater. Pavement Des.* **2004**, *5*, 9–24. [CrossRef]
7. Wu, S.-p.; Zhu, G.-j.; Chen, Z.; Liu, Z.-f. Laboratory research on rheological behavior and characterization of ultraviolet aged asphalt. *J. Cent. South Univ. Technol.* **2008**, *15*, 369–373. [CrossRef]
8. Zhang, H.; Wang, H.; Yu, J. Effect of aging on morphology of organo-montmorillonite modified bitumen by atomic force microscopy. *J. Microsc.* **2011**, *242*, 37–45. [CrossRef]
9. Lyne, Å.L.; Wallqvist, V.; Rutland, M.W.; Claesson, P.; Birgisson, B. Surface wrinkling: The phenomenon causing bees in bitumen. *J. Mater. Sci.* **2013**, *48*, 6970–6976. [CrossRef]
10. Jun, Y.; Minghui, G.; Troy, P.; Jianming, W.; Xiaoting, W. Study on micro-structures of asphalt by using atomic force microscopy. *Acta Pet. Sin. (Pet. Process. Sect.)* **2015**, *31*, 959–965. [CrossRef]
11. Pauli, A.; Grimes, R.; Beemer, A.; Turner, T.; Branthaver, J. Morphology of asphalts, asphalt fractions and model wax-doped asphalts studied by atomic force microscopy. *Int. J. Pavement Eng.* **2011**, *12*, 291–309. [CrossRef]
12. Das, P.K.; Kringos, N.; Wallqvist, V.; Birgisson, B. Micromechanical investigation of phase separation in bitumen by combining atomic force microscopy with differential scanning calorimetry results. *Road Mater. Pavement Des.* **2013**, *14*, 25–37. [CrossRef]
13. Das, P.K.; Kringos, N.; Birgisson, B. Microscale investigation of thin film surface ageing of bitumen. *J. Microsc.* **2014**, *254*, 95–107. [CrossRef] [PubMed]
14. Xiaoyi, P. Asphalt and Aggregate Adhesion Characteristics Analysis Based on the Principle of AFM and the Surface Energy. Master's Dissertation, Harbin Institute of Technology, Harbin, China, 2015.
15. Ben, L.; Ju-nan, S.; Peng-cheng, S. Nano-scale microscopic characteristics and functional groups of aged asphalt. *J. Highw. Transp. Res. Dev.* **2016**, *33*, 6–13. [CrossRef]
16. Lyne, Å.; Wallqvist, V.; Birgisson, B. Adhesive surface characteristics of bitumen binders investigated by Atomic Force Microscopy. *Fuel* **2013**, *113*, 248–256. [CrossRef]
17. Van Oss, C.J. *Interfacial Forces in Aqueous Media*; CRC Press: Boca Raton, FL, USA, 2006.

18. Van Oss, C.; Giese, R. Surface modification of clays and related materials. *J. Dispersion Sci. Technol.* **2003**, *24*, 363–376. [CrossRef]
19. Della Volpe, C.; Siboni, S. Some reflections on acid-base solid surface free energy theories. *J. Colloid Interface Sci.* **1997**, *195*, 121–136. [CrossRef]
20. Della Volpe, C.; Siboni, S. Acid-base surface free energies of solids and the definition of scales in the Good-van Oss-Chaudhury theory. In Proceedings of the International Symposium on Apparent and Microscopic Contact Angles in Conjunction with the 216th American-Chemical-Society Meeting, Boston, MA, USA, 24–27 August 1998; pp. 171–208.
21. Yingying, D.; Xiaomin, L.; Zhijie, Y.; Dingbang, W. Adhesion and water stability of pegenerated asphalt based on surface free energy. *J. Mater. Sci. Eng.* **2020**, *38*, 648–653. [CrossRef]
22. Gan, X.; Zhang, W. Application of biochar from crop straw in asphalt modification. *PLoS ONE* **2021**, *16*, e0247390. [CrossRef] [PubMed]
23. Zhen, Y. Study on Multi-Scale Behavioral Characteristics of Asphalt before and after Aging. Master's Dissertation, South China University of Technology, Guangzhou, China, 2018.
24. Wu-ping, R.; Shan-shan, Z.; Hai-lin, Z.; Ling, L.; Yu, Z. Stability of asphalt mortar from pyrolysis residue of oil sludge modified with hydrated lime based on rheological properties. *China J. Highw. Transp.* **2023**, *36*, 107–119. [CrossRef]
25. Qingfu, Z.; Zhi-min, W.; Bao-guo, C.; Gui-feng, L.; Ji, Z. Analysis of XRD spectral structure and carbonization of the biochar preparation. *Spectrosc. Spectral Anal.* **2016**, *36*, 3355–3359. [CrossRef]
26. Loeber, L.; Sutton, O.; Morel, J.; Valleton, J.M.; Muller, G. New direct observations of asphalts and asphalt binders by scanning electron microscopy and atomic force microscopy. *J. Microsc.* **1996**, *182*, 32–39. [CrossRef]
27. Minda, R. Study on Modification Mechanism and Micro-Properties of Poly-Phosphoric Acid Modified Asphalt Considering Aging Performance Base on AFM. Master's Dissertation, Inner Mongolia University of Technology, Inner Mongolia, China, 2018.
28. Lageng, S.; Gaochao, W.; Er-hu, Y. Research on surface energy of asphalt based on atomic force microscope. *J. China Foreign Highw.* **2018**, *38*, 287–289. [CrossRef]
29. Young, T.; Monclus, M.; Burnett, T.; Broughton, W.; Ogin, S.; Smith, P. The use of the peak force TM quantitative nanomechanical mapping AFM-based method for high-resolution Young's modulus measurement of polymers. *Meas. Sci. Technol.* **2011**, *22*, 125703. [CrossRef]
30. Little, D.N.; Bhasin, A. *Using Surface Energy Measurements to Select Materials for Asphalt Pavement*; Transportation Research Board: Washington, DC, USA, 2007.
31. Yunqing, G.; Licheng, D.; Ze, Y.; Xu, Z. Research on misalignment fault diagnosis method for rotating machinery based on pearson correlation coefficient. *New Technol. New Prod. China* **2022**, 48–50. [CrossRef]
32. Cheng, D. *Surface Free Energy of Asphalt-Aggregate System and Performance Analysis of Asphalt Concrete Based on Surface Free Energy*; Texas A&M University: College Station, TX, USA, 2002.
33. Wei, J. Study on Surface Free Energy of Asphalt, Aggregate and Moisture Diffusion in Asphalt. Ph.D. Thesis, China University of Petroleum, Beijing, China, 2008.
34. Zhu, J.; Zhang, K.; Liu, K.; Shi, X. Adhesion characteristics of graphene oxide modified asphalt unveiled by surface free energy and AFM-scanned micro-morphology. *Constr. Build. Mater.* **2020**, *244*, 118404. [CrossRef]